

Enabling Long-term Cycling Stability of $\text{Na}_3\text{V}_2(\text{PO}_4)_3/\text{C}$ vs. Hard Carbon Full-cells

Pirmin Stüble,^{*[a]} Cedric Müller,^[a] Julian Klemens,^[b] Philip Scharfer,^[b] Wilhelm Schabel,^[b] Marcel Häringen,^[a] Joachim R. Binder,^[a] Andreas Hofmann,^[a] and Anna Smith^{*[a]}

Sodium-ion batteries are becoming an increasingly important complement to lithium-ion batteries. However, while extensive knowledge on the preparation of Li-ion batteries with excellent cycling behavior exists, studies on applicable long-lasting sodium-ion batteries are still limited. Therefore, this study focuses on the cycling stability of batteries composed of $\text{Na}_3\text{V}_2(\text{PO}_4)_3/\text{C}$ based cathodes and hard carbon anodes. It is shown that full-cells with a decent stability are obtained for ethylene carbonate-propylene carbonate electrolyte and the conducting salt NaPF_6 . With cathode loadings of $1.2 \text{ mAh}/\text{cm}^2$, after cell formation discharge capacities up to 92.6 mAh/g are

obtained, and capacity retentions $>90\%$ over 1000 charge/discharge cycles at $0.5 \text{ C}/0.5 \text{ C}$ are observed. It is shown that both, the additive fluoroethylene carbonate and impurities in the electrolyte, negatively affect the overall discharge capacity and cycling stability and should therefore be avoided. Remarkably, the internal resistances of well-balanced and well-built cells did not increase over 1500 cycles and 5 months of testing, which is a very promising result regarding the possible lifespan of the cells. The initial loss of active sodium ions in hard carbon remains a major problem, which can only be partially reduced by proper balancing.

Introduction

$\text{Na}_3\text{V}_2(\text{PO}_4)_3$ (NVP) is long known to battery research, although, for nearly a decade it was merely considered as a precursor for cathode materials for lithium-ion batteries (LIBs) like, e.g., $\text{Li}_2\text{NaV}_2(\text{PO}_4)_3$, which was accessible exclusively through cation exchange reactions.^[1] The use as an electrode material for sodium-ion batteries (SIBs) came into focus around 2010^[2] and considerable progress was made when it was found that the issue of low electronic conductivity could be addressed by carbon coatings.^[3] Common notations indicating the carbon content of such NVP composite material include NVP/C or NVP@C. In 2013, it was finally demonstrated that stable cycling

can be achieved when using NVP/C cathode active material together with sodium metal anodes.^[4]

NVP itself crystallizes in the so-called NaICON (Na^+ Superlonic Conductor) structure-type in space group $R\bar{3}\text{cH}$. Two sodium ions occupying the $18b$ site of NVP can be extracted leading to the formal composition $\text{Na}_1\text{V}_2(\text{PO}_4)_3$. The mobilization of the remaining sodium cation from Wyckoff site $6b$ is not possible within the stability range of common electrolytes^[1,5,6] and, to the best of our knowledge, a fully de-sodiated state has not been reported so far. But besides extracting sodium ions, it is also possible to insert additional sodium ions into the crystal structure of NVP. The insertion of a fourth Na^+ is observed at $\sim 1.6 \text{ V}$ (vs. Na/Na^+)^[3] and a fifth sodium can be inserted at $\sim 0.3 \text{ V}$ (vs. Na/Na^+), leading to the composition $\text{Na}_5\text{V}(\text{PO}_4)_3$.^[7] Even higher sodiation states like $\text{Na}_6\text{V}(\text{PO}_4)_3$ have also been reported and discussed.^[8]

For practical application in a SIB, however, sodiation levels of $1 \leq x \leq 4$ in $\text{Na}_x\text{V}_2(\text{PO}_4)_3$ are of particular importance. When functioning as a cathode, common voltage windows like 2.3 to 3.9 V ,^[9] cover $\text{V}^{III}/\text{V}^IV$ redox activity with the formal reaction $\text{Na}_3\text{V}_2^{III/II/III}(\text{PO}_4)_3 \rightleftharpoons \text{Na}_2\text{V}_2^{III/IV}(\text{PO}_4)_3 \rightleftharpoons \text{NaV}_2^{IV}(\text{PO}_4)_3$ at roughly 3.4 V (vs. Na/Na^+), corresponding to a specific capacity of 116.6 mAh/g . When cycling against Na metal anodes, the capacity can easily be increased by reducing the lower voltage limit, e.g. to 1.2 V . During discharge, the fourth Na^+ is inserted according to $\text{Na}_3\text{V}_2^{III/II/III}(\text{PO}_4)_3 + \text{Na}^+ + \text{e}^- \rightleftharpoons \text{Na}_4\text{V}_2^{II/III}(\text{PO}_4)_3$, leading to a partial reduction of vanadium to $\text{V}(\text{II})$ and an increase of the capacity to 174.9 mAh/g (based on the molar mass of N_3VP). However, while a fourth Na^+ leads to a capacity increase by 50%, the energy density increases by only about 22% due to the lower voltage of the $\text{V}(\text{II})/\text{V}(\text{III})$ redox step. Additionally, the insertion of the fourth Na^+ occurs along with an additional two phase reaction,^[3,10] which can lead to accelerated degradation of the NVP active material.^[9]

[a] Dr. P. Stüble, C. Müller, Dr. M. Häringen, Dr. J. R. Binder, Dr. A. Hofmann, Dr. A. Smith

Institute for Applied Materials (IAM)

Karlsruhe Institute of Technology (KIT)

Hermann-von-Helmholtz-Platz 1, 76344 Eggenstein-Leopoldshafen (Germany)

E-mail: pirmin.stueble@kit.edu

anna.smith@kit.edu

Homepage: <https://www.iam.kit.edu/ess/english/1192.php>

[b] J. Klemens, Dr.-Ing. P. Scharfer, Prof. Dr.-Ing. W. Schabel

Thin Film Technology (TFT)

Karlsruhe Institute of Technology (KIT)

Straße am Forum 7, 76131 Karlsruhe (Germany)

Supporting information for this article is available on the WWW under <https://doi.org/10.1002/batt.202300375>

This publication is part of a joint Special Collection dedicated to Post-Lithium Storage, featuring contributions published in Advanced Energy Materials, Batteries & Supercaps, and ChemSusChem.

© 2023 The Authors. Batteries & Supercaps published by Wiley-VCH GmbH. This is an open access article under the terms of the Creative Commons Attribution Non-Commercial NoDerivs License, which permits use and distribution in any medium, provided the original work is properly cited, the use is non-commercial and no modifications or adaptations are made.

It is a peculiarity of SIBs, that graphite based anodes, that are state of the art electrodes in commercial LIBs, cannot be used due to limited solvent-free intercalation ability of sodium between graphite layers.^[11] Hard Carbon (HC) is commonly used instead, which is challenging and advantageous at the same time. On the positive side, compared to graphite, HC has an abundant choice of precursors and a good perspective for the reduction of production cost and environmental impact.^[12] HC is therefore regarded as the most promising candidate for anode materials in commercial SIBs.^[12,13] One the negative side, however, the initial capacity loss of HC during battery formation is still higher than for graphite-based anodes in state of the art LIB-systems.^[14] On both, graphite and HC, a solid electrolyte interface (SEI) is formed in which some of the charge carriers are bound. However, in HC in addition there is a significant amount of defects and oxygen functionalities where additional sodium remains irreversibly trapped.^[15] As a consequence, proper balancing of the capacity ratio of negative to positive electrode (N/P ratio), is crucial. The areal capacity of the HC anode should slightly exceed the capacity of the cathode in order to avoid sodium plating and dendrite formation. Simultaneously, the capacity of the anode should not be significantly higher or overbalanced, as this leads to even higher losses of electrochemically active sodium from the cathode during cell formation and thus to a loss of capacity and with that energy density of the battery cell. To address the issue of irreversible sodium loss, promising pre-sodiation strategies for SIBs with HC anodes have recently been developed, e.g. by using Na-biphenyl,^[10] Na₂C₂O₄,^[16] or Na₄C₄O₄.^[17] However, to the best of our knowledge, such pre-sodiation strategies have so far only been implemented on a laboratory scale.

With vanadium, NVP contains a rare and expensive transition metal, which currently reduces the perspective of large-scale application.^[18] However, the possibility of recovering and reusing vanadium to a large extent, as required by current regulatory frameworks for batteries,^[19] could increase the attractiveness and sustainability of the system. Another prerequisite to compensate for these disadvantages, would be the possibility to build exceptionally stable and long-lasting cells, to which this paper is meant to contribute. While there are already a number of studies with very promising cycling stabilities for symmetric NVP/C vs. NVP/C cells or NVP/C vs. Li half-cells,^[4,20,21] where 10000 cycles and more were realized, the number of studies on NVP/C vs. HC full-cells is quite limited and the cell degradation remains a major obstacle.^[5,22] Figure 1 shows the capacity retention of NVP/C vs. HC full-cells against the number of cycles reported in literature. More detailed information on the individual studies is given in Table S1. It becomes obvious that numerous studies report quite different lifetimes for NVP/C vs. HC cells, which may be largely due to different electrolytes, loadings and C-rates, or possibly also due to external factors such as cell assembly, which – especially in the case of coin cells – has an enormous influence on the long term cycling stability.^[23] The cause of the capacity decay in full-cells has been investigated previously.^[10] Herein, loss of active sodium to the solid electrolyte interface (SEI) is reported to lead to a decrease of the overall capacity of the NVP/C vs. HC cells. The same study

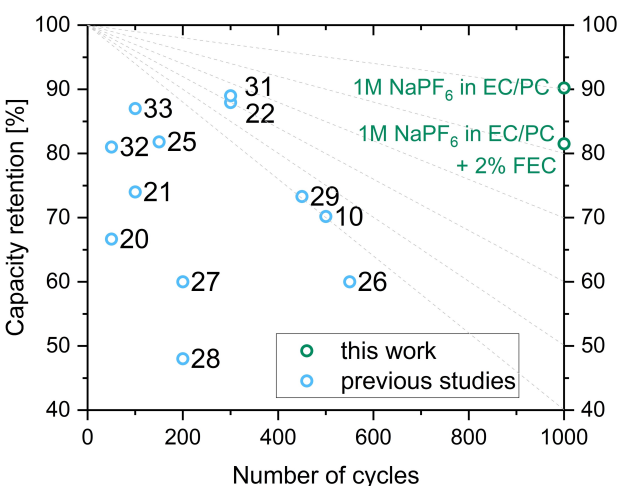


Figure 1. Cycling stability of NVP/C vs. HC full-cells in previously published studies,^[10,20–22,25–29, 31–33] compared to the present work. Further experimental information (if available) are summarized in Table S1.

reports an almost full recovery of the NVP/C capacity when cycled against fresh sodium. This mechanism for capacity loss is by no means new or unusual, but is also well documented for LIBs, as recently shown in a study on long-term stable LiNi_{0.5}Mn_{1.5}O₄ vs. graphite full-cells.^[24] Although we were not yet able to completely prevent capacity loss, with this study, we would like to show how NVP/C vs. HC full-cells with a very promising cycling stability can be prepared. These results may be considered as a starting point for further improvement, e.g. through more adequate electrolytes, the use of additives, pre-sodiation strategies and by using more appropriate long-term stable cell formats, such as pouch cells.

Unfortunately, it becomes obvious that data reported in the literature is difficult to compare. Information was extracted on the cell format, electrode size, separator, electrode loading, electrolyte, balancing factor electrode formulation, loading, and C-rate and the corresponding values are listed in Table S1. However, most publication lack in one or multiple information on key data and in certain cases, values can be estimated, but not precisely stated.

Experimental

Preparation of the NVP/C Composite Material

Similar to previous works,^[20] the NVP/C composites were synthesized via a two-step spray-drying process. Na₂CO₃, NH₄H₂PO₄, NH₄VO₃ and β-lactose in a molar ratio of 1:2:1.3:0.7 were dissolved in water at 73 °C and spray dried in a MobileMinor spray drier (GEA) with an inlet and outlet temperature of 210 °C and 112 °C, respectively. In order to decompose the precursor, the powder obtained was calcined in a CWF 63 furnace (Carbolite Gero). At a rate of 60 K/h, the precursor was heated to 450 °C and held for 2 h. Subsequently, with a rate of 180 K/h, the furnace was further heated to 850 °C, held for 5 h and then cooled to room temperature at a cooling rate set to 300 K/h. Below approximately 500 °C actual cooling rates were slower due to the lack of active cooling. The whole thermal process was carried out under argon atmosphere.

The resulting pre-calcined powder was crushed in a mortar grinder and then ground in a ball mill with ZrO_2 grinding balls ($\phi: 0.2\text{ mm}$). Before the second spray drying process with the same inlet and outlet temperatures, a solution of polyacrylic acid ($M_n=1800$, 10.1 g/L) and polyethylene glycol ($M_n=400$, 0.9 g/L) was added. The powder obtained was calcined again in the same furnace, which was heated to 800°C with 180 K/h and held for 5 h in an Ar–H atmosphere (97:3 wt%) with continuous gas flow. The resulting NVP/C composite was crushed with a mortar grinder and sieved with a 32 μm sieve. By means of mercury intrusion porosimetry, the porosity inside the NVP/C granules was determined to be 36.8% at a major pore width of 15 nm. The evaluation of nitrogen adsorption isotherms according to the Brunauer–Emmett–Teller theory yielded a specific surface area of $95.5\text{ m}^2/\text{g}$. The carbon content was determined to be 9.8% by means of elemental analysis.

Electrode preparation

The electrodes investigated originate from large-scale processing and are based on processes originally developed for LIB technology.^[34,35] A detailed description focusing on NVP/C processing was recently provided by Klemens *et al.*^[36] and here we briefly summarize the process. The slurry for NVP/C cathodes was mixed in a dissolver (Dispermat SN-10, VMA Getzmann), where carbon black (C65, C-Nergy) and graphite (KS6L, Timcal-Imerys), a PVDF (Solef 5130, Solvay) binder-solvent solution with 7.5 wt% and about 50% of the required amount of NMP were dispersed. The NVP/C composite material and remaining NMP were added to the dispersed PVDF/NMP and conductive additive slurry to adjust the solid content to 50 wt%. Vacuum was applied to remove existing gases from the slurry. The slurries for the HC electrodes were prepared accordingly, but in an aqueous process. The conductive additive Super C65 (Imerys) and a MAC500LC (Nippon Paper) carboxymethyl cellulose (CMC) binder-solvent solution with 2 wt% were dispersed. HC (Kuranode Type II, 9 μm , Kuraray) and additional water were added. In a last mixing step, an aqueous solution of styrene-butadiene rubber (SBR, 40 wt%, Zeon Europe) was added to adjust the final solid content to 43 wt%. The electrode coating and drying was carried out under quasi-isothermal drying conditions as a discontinuous process likewise described by Klemens *et al.*^[34–36] The slurries were applied to an aluminum current collector by a doctor blade (ZUA 2000.60, Zehntner) and dried by an impingement dryer and temperature controlled heating plates, resulting in drying rates of $0.75\text{ g m}^{-2}\text{ s}^{-1}$ in both cases. After drying, the electrodes were calendered at 50°C . The composition of the cathode and anode results as 90.5 wt% NVP/C, 3 wt% C65, 2 wt% KS6 L and 4.5 wt% PVDF and 93 wt% HC, 1.4 wt% C65, 1.87 wt% CMC, 3.73 wt% SBR, respectively.

Electrolyte preparation

Electrolytes A and A+FEC were prepared in an argon filled glovebox (MBraun) with oxygen and water levels below 0.5 ppm. Ethylene carbonate (EC, Gotion, 99.9%) and propylene carbonate (PC, Gotion, 99.9%) were used as electrolyte solvents in a mass ratio of 1:1. The conducting salt $NaPF_6$ (1 M, CHEMFISH TOKYO CO., LTD, 99.9%) and, if necessary, fluoroethylene carbonate (FEC, Gotion, 99.9%) were added in a plastic 10 mL volumetric flask for precise preparation of 1 mol/L conducting salt concentration. The electrolytes were then stored in 10 mL aluminum vials due to the incompatibility of $NaPF_6$ and FEC with glass surfaces.

Electrolyte B was prepared analogously in a different argon filled Glovebox ($O_2 < 0.1\text{ ppm}$, $H_2O < 0.1\text{ ppm}$). EC (Sigma Aldrich, 99%) was similarly mixed with PC (Sigma Aldrich, 99.7%) in a mass ratio

of 1:1 and a 1 M $NaPF_6$ (Alfa Aesar, 99%) solution was prepared. The water content of electrolytes A and B was determined by means Karl Fischer titration (C30, Mettler Toledo).

Half-cell tests

In order to determine capacity of the HC anode and the NVP/C cathode, electrodes were investigated with sodium metal counter and reference electrodes in a three-electrode setup, which was recently presented and discussed in detail by Müller *et al.*^[37] Briefly summarized, it enables accurate and reliable determination of active material capacities even for highly loaded electrodes and minimizes errors originating from potential fluctuations, which is crucial especially in the case of HC. The electrodes and separators (GF/D, Whatman) were dried at 120°C under vacuum overnight, cell parts and gaskets were dried at 80°C before being transferred into the glovebox. Cells were assembled in a glove box under argon atmosphere (water $< 0.1\text{ ppm}$, oxygen $< 0.1\text{ ppm}$). Two separators were placed between working electrode and counter electrode, one separator was placed in front of the reference electrode. Electrolyte A+FEC was used. Before cycling, the cells rested overnight at room temperature. As stated in Table S2, four constant current (CC) charge and discharge cycles at 0.05 C were then executed in the potential range of 2.3 to 3.9 V (NVP/C cathode vs. sodium reference electrode) and 2 V to 5 mV (HC anode vs. sodium reference electrode). Details on the electrodes are given below.

Full-cell tests

NVP/C and HC electrode disks (both $\phi: 16\text{ mm}$) were punched out and dried overnight under vacuum at 120°C . NVP/C vs. HC full-cells were then assembled as CR2032 coin cells in an argon filled glove box, using Whatman QMA glass fiber separator ($\phi: 16.5\text{ mm}$) and 110 μL of electrolyte and a spacer disk with a thickness of 1 mm. To calculate the precise N/P ratio later on, electrodes were weighted prior to their use. It has recently been shown that the steel grade of coin cell cases can have an enormous impact on the cycle life of alkali-ion batteries cycled vs. carbon-based anodes^[23] and accordingly, coin cell parts made of S316L steel were chosen. After crimping, the cells were cleaned to remove any electrolyte deposits and possible salt bridges. Before testing, the cells rested for 12 hours at 25.0°C to allow the electrolyte to soak into the pores of the electrodes. Cycling then was executed at the same temperature within a climate chamber. All cell tests were performed within the voltage window of 2.3 to 3.9 V. For cell formation, four full cycles with charge and discharge rates of 0.05 C were completed (cf. Table S2). After the 4th formation cycle, the cells were charged to 3.5 V to avoid a pause in the discharged state. A rate capability test only was performed with some selected cells. As listed in Table S3, the charge rate was kept constant at 0.5 C and each two cycles with discharge rates of 0.5 C, 1 C, 2 C, 3 C, 4 C and 5 C were passed. In order to verify that no test related damage was dealt, two more test cycles with a discharge rate of 0.5 C were added. To investigate the long-term cycling stability, for all cells a combined test protocol containing check-up cycles, after each 100 charge-discharge cycles, with direct current internal resistance (RiDC) measurements at different states of charge (SOC) was used. Herein, the cells were charged and discharged at 0.1 C. The discharge capacity obtained was used to calculate the capacities corresponding to a SOC of 10%, 30%, 50%, 70% and 90%, which then were used as measuring points for the RiDC test in the subsequent charging cycle. For the latter, a 20 second pulse with a C-rate of 1 C was applied. In order not to falsify the subsequent measurements, the discharged capacity during the RiDC pulse was compensated. Then the cell again was discharged with 0.5 C. After these check-up

Table 1. General properties of the electrodes investigated. Mean values and standard deviations (in brackets). Specific capacities were determined in half-cell configuration using sodium anodes. Electrode thicknesses were calculated before/after calendering. For details of the determination of the specific capacity, see below.

Label	Active material (AM)	Electrode properties					
		Type	Specific capacity [mAh/g]	AM content [wt %]	AM loading [mg/cm ²]	Areal capacity [mAh/cm ²]	Electrode thickness [μm]
NVP-1	Na ₃ V ₂ (PO ₄) ₃		111.3	81.6	11.1(3)	1.23(3)	136(4)/105(2)
HC-1	Hard Carbon		341.1	93	4.2(2)	1.43(5)	60(5)/57(2)
HC-2	Hard Carbon		341.1	93	7.0(2)	2.39(6)	96(5)/84 (2)

cycles, 100 charge discharge cycles with a constant current constant voltage (CCCV) charging step at 0.5 C (with CV phase until $I < 0.05$ C) and CC discharge step at 0.5 C were executed. Hereafter, new check-up cycles and the next 100 charge discharge cycles followed, resulting in total test times of roughly 3 to 6 months for 1500 cycles.

Statistical analysis

The average loadings of the electrodes were determined based on the weight each 7 individual electrode discs ($\varnothing = 16$ mm) for NVP/C, HC-1 and HC-2, respectively, see Table 1. The electrode thicknesses before and after calendering were determined by 4 single point measurements. The coin cell tests were verified using at least two identically prepared cells, which in all cases showed very similar cycling behavior and the better performing cell is shown. In the case of cell 4 (overbalancing of the anode + FEC), the second cell test failed, so that only a single and therefore less reliable data set is available. This, however is pointed out again in the discussion below.

Results and Discussion

Electrode and electrolyte properties

General properties of the NVP/C cathode (NVP-1) and the two differently loaded HC anodes (HC-1 and HC-2) investigated are listed in Table 1. As described above, pure NVP lacks electronic conductivity for its application in batteries. Therefore, NVP/C composite materials are used, where carbon-containing precursors are added during synthesis in order to increase the electronic conductivity. Accordingly, both the proportion of NVP in the NVP/C composite material (90.2 wt %) and the proportion of the NVP/C composite material in the cathode layer (90.5 wt %) must be taken into account to calculate the overall NVP content in the cathode layer (81.6 wt %). Based on this value, the loading of the pure NVP in the cathode, was determined to be 11.1(4) mg/cm² which corresponds to an areal capacity of 1.23(3) mAh/cm², based on a specific capacity of 111.3 mAh/g for NVP (details see below). The two anodes HC-1 and HC-2 contain 93 wt % of the HC active material. In good agreement with a previous study,^[37] the specific capacity of HC was determined to be 341.1 mAh/g² (see below). Accordingly, the average HC loadings were determined to be 4.2(2) and 7.0(2) mg/cm² corresponding to areal capacities of 1.43(5) and

2.39(6) mAh/cm². In all cells investigated, the HC anodes were overbalanced compared to NVP and no evidence of Na-plating was found during the investigation. The higher loadings of hard carbon were investigated in order to reliably estimate the additional sodium loss during formation and to investigate possible impacts on the N/P ratio on the long-term cycling stability of the cells. In addition, the overbalancing of hard carbon could also offer a way out of the dilemma that the available HC capacity via CC charging decreases significantly with increasing C-rate,^[37] which limits the fast charging capability of full-cells with a N/P ratio close to 1. Based on the areal capacities mentioned before, and the circumstance that electrode discs with the same diameter (16 mm) were used, the N/P ratio of the NVP-1 cathode vs. the HC-1 anode is roughly 1.2, while NVP-1 vs. HC-2 yields a N/P ratio of 1.9. However, electrode masses and the resulting N/P ratio was determined for each cell individually and the corresponding values are listed in Table 3.

An overview of the electrolytes used during this investigation is given Table 2. 1 M NaPF₆ in EC/PC and the optional addition of FEC was chosen on the basis of previous studies^[38] and preliminary screening of the electrolyte stabilities against sodium metal.^[37] The water content of electrolyte A was determined to be below 10 ppm by means of Karl-Fischer titration. The water content of the electrolyte A + FEC was not determined separately. However, based on the voltage profiles of the first charging step (cf. Figures 3 and 7), it becomes evident that FEC and trace water have distinguishable effects. Therefore, it is very unlikely that an artifact from trace water introduced with FEC is seen instead of an effect of FEC. Electrolyte B was prepared in another Glovebox, with EC and PC and NaPF₆ originating from different suppliers (details see experimental section). The water content of electrolyte B was determined to be 60 ppm. However, as significantly lower

Table 2. Composition and water content of electrolytes used in full-cells.

Electrolyte	Composition	Water content
A	1 M NaPF ₆ in EC/PC (w/w)	< 10 ppm
A + FEC	1 M NaPF ₆ in EC/PC (w/w) + 2 wt% FEC	not determined, presumably similar to A
B	1 M NaPF ₆ in EC/PC (w/w)	60 ppm

values were measured in the corresponding batches of EC and PC, the source of moisture presumably was the conducting salt NaPF₆. In case of electrolyte B, the latter may not always have been handled correctly, and was not dried before use.

NVP/C and HC vs. sodium half-cells

The potential profiles of the formation cycles of a NVP-1 cathode cycled against a sodium metal anode at 0.05 C are shown in Figure 2(a). The discharge capacities of the formation cycles hardly deviate (<0.1 mAh/g) and were determined to be 111.3 mAh/g when referring to the pure NVP active material. Taking into account the carbon content of NVP/C (9.8 wt%), a reduced composite material capacity of 100.4 mAh/g is obtained.

The specific charge capacity of the hard carbon material used in this study was determined to be 341.1 mAh/g based on three-electrode investigations of HC-1 vs sodium metal working and reference electrodes in the potential range of 5 mV to 2 V (HC vs. reference electrode) at a C-rate of 0.05 C (cf. Figure 2b). The profile of the first charge cycle of HC deviates significantly from the subsequent charge cycles. Charge capacities in cycles 2 to 4 are reduced to 282.9 to 279.8 mAh/g. This behavior is typical for hard carbon and is attributed mainly to the irreversible binding of sodium on defect sites and oxygen functionalities in HC. However, especially in the case of hard carbon materials with a large specific surface area, SEI formation can likewise significantly contribute to initial capacity loss.^[15] The investigation of HC-1 nevertheless yields almost the same specific capacity, as previously reported for investigations of slightly higher loaded electrodes with the same formulation and same hard carbon material (335 mAh/g).^[37] The discharge capacity of HC slightly increases with the formation cycle number, starting from 264.7 mAh/g and reaching 269.7 mAh/g in the fourth cycle, which is likewise in perfect agreement with previous investigations.^[37] For the full-cell design and balancing

of the cells, the charge capacity of the first cycle is the decisive value. A detailed discussion the capacity of highly loaded HC anodes, investigations of the rate-dependent capacity, and further investigations can be found in a separate work by C. Müller *et al.*^[37]

NVP/C vs. HC full-cells

Cell formation

The formation cycles of the NVP/C vs. HC full-cells containing electrolyte A and A+FEC are shown in Figure 3. The charge capacities of the first cycles are in the range of 110.8 to 111.7 mAh/g and, thus, are in very good agreement with the active material capacity of 111.3 mAh/g determined in the half-cell. This indicates that even during the first charge cycle, virtually all side reactions involve sodium from the NVP active material. Pure voltage-induced oxidation reactions of the electrolyte, in contrast, do not seem to occur in the voltage window of 2.3 to 3.9 V. In this regard, NVP/C vs. HC clearly seems to differ from high voltage (LIB) systems, where additional oxidation reactions occur during SEI formation and the charge capacity of the first cycle significantly exceeds the discharge capacity of the active material, as observed for instance for LNMO vs. graphite cells.^[24]

As discussed above, the discharge capacities of the full-cells with hard carbon anodes are significantly reduced compared to the half-cells as a result to irreversible capacity losses in the first cycle. Based on the current knowledge, this capacity loss can mainly be attributed to defect sites and oxygen functionalities of hard carbon, where sodium is trapped.^[15] A peculiarity in the charge profiles of the FEC containing cells is an additional step around 2.5 to 2.7 V, which is encircled in Figure 3 and which indicates slightly different formation processes. For sodium vs. hard carbon cells, it was shown that FEC promotes the formation NaF on the surface of hard carbon,^[39] which might be

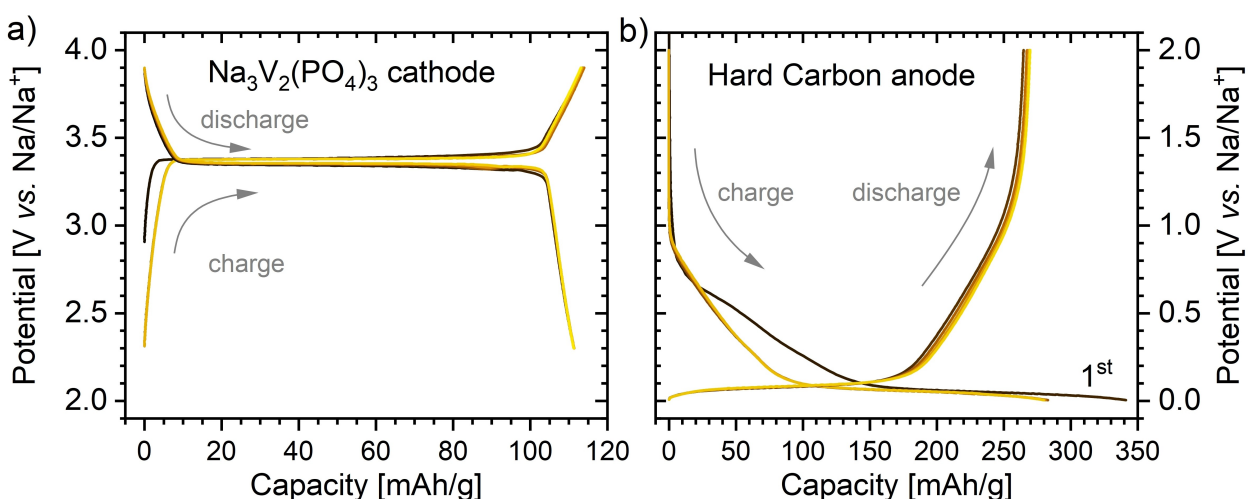


Figure 2. Voltage profiles of the formation cycles of a) a NVP/C vs. Na half-cell and b) a HC vs. Na half-cell at 0.05 C. Lighter colors indicate increasing cycling time. As electrolyte, 1 M NaPF₆ in EC/PC (w/w) + 2 wt% FEC was used.

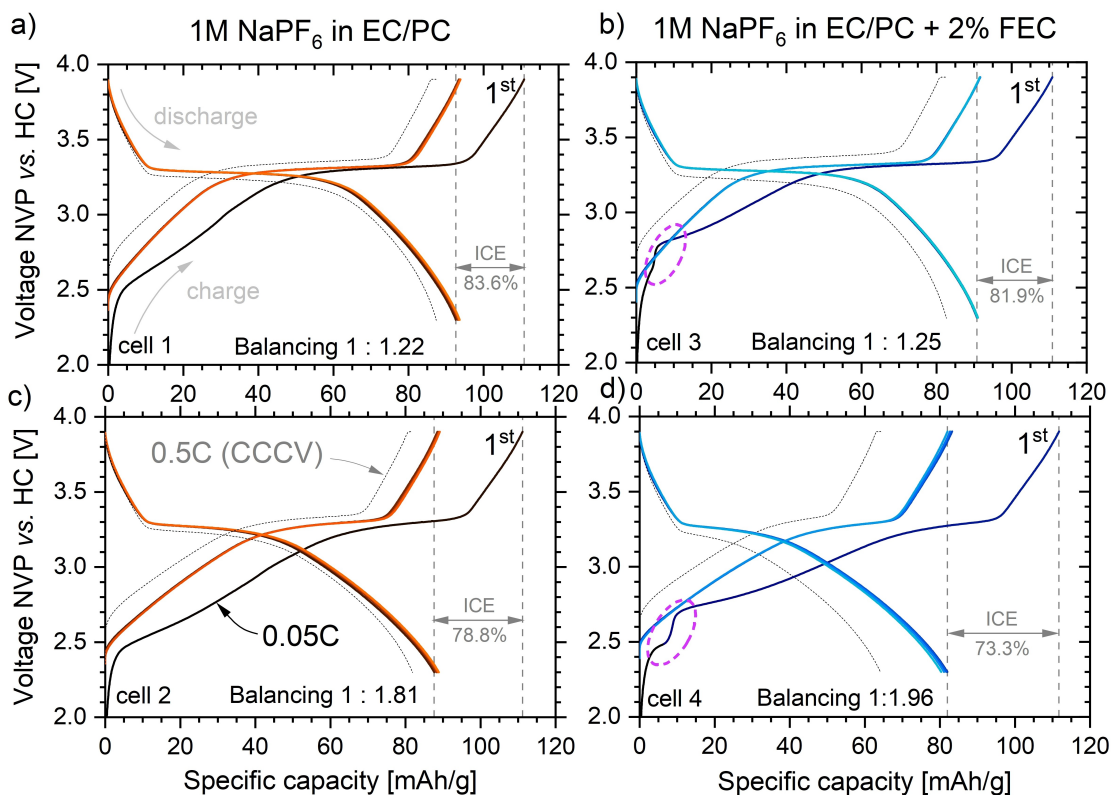


Figure 3. Voltage profiles of the formation cycles of NVP/C vs. HC full-cells with a, b) well balanced and c, d) overbalanced anodes at a C-rate of 0.05 C. Electrolyte A a, c) without and b, d) with the additive FEC was used. The presumably FEC-specific redox stages in the first charging step are highlighted by pink circles. For comparison, the first full cycle with 0.5 C is represented by the dotted lines. Specific capacities refer to mass of pure NVP.

a plausible explanation for additional loss of sodium in the FEC containing cells compared to the FEC-free cells.

The individual values of the first cycle discharge capacity during the formation cycles are listed in Table 3 and range from 92.6 to 82.0 mAh/g. During the subsequent formation cycles, there is comparatively little variation in the voltage profiles. In the FEC-free cells, the discharge capacity slightly increases, to 93.3 and 88.9 mAh/g (cells 1 and 3). In the FEC containing, discharge capacities remain almost the same (91.0 mAh/g, cell

2) or slightly decrease to 80.3 mAh/g for cell 4 at the end of the last formation cycle. Hence, from Figure 3 it becomes obvious that the initial loss is influenced by both, NVP vs. HC balancing and the use of FEC. The initial coulombic efficiency (ICE) in the cells with the additive FEC is reduced by roughly 2 and 5% when comparing the cell 1 vs. 3 and cell 2 vs. 4, respectively. For higher N/P ratios, the ICE reduction was found to be 5% and 9% (cell 1 vs. 2 and cell 3 vs. 4).

Table 3. Overview of the cells investigated in this study. For the calculation of the areal capacities and the resulting N/P ratio, specific capacities of 111.3 mAh/g and 335.0 mAh/g for NVP and HC were assumed. Cells 1–4 were built to investigate the impact of FEC and the balancing. Cells 5 and 6 were built 3 months later for an additional investigation of the impact of moisture and electrolyte quality. Discharge capacities refer to the mass of pure NVP. The results were confirmed by at least one identically built reference cell. *In the case of cell 4, the reference cell test failed, so that only one (less reliable) data set is available.

Cell	Cathode		Anode		Balancing N/P ratio	Electrolyte	Discharge capacity			
	Type	Areal capacity [mAh/cm ²]	Type	Areal capacity [mAh/cm ²]			0.05 C [mAh/g]	0.5 C [mAh/g]		
1	NVP-1	1.28	HC-1	1.57	1.22	A	92.6	87.8		
2	NVP-1	1.29	HC-2	2.34	1.81	A	87.6	82.2		
3	NVP-1	1.20	HC-1	1.51	1.25	A + FEC	90.8	83.0		
4*	NVP-1	1.19	HC-2	2.32	1.96	A + FEC	82.0	64.7		
5	NVP-1	1.27	HC-1	1.52	1.20	A	90.1	87.4		
6	NVP-1	1.22	HC-1	1.49	1.23	B	85.8	80.8		

For the sake of completeness, the first charge and discharge cycle of the continuous cycling (0.5 CCCV/0.5 C) are also shown in Figure 3 (thin dashed lines). Compared to the formation cycles (0.05 C), in the FEC containing cells, significantly lower capacities are available at 0.5 C than in cells without additive. This could be the result of higher resistance of the SEI, as discussed below, but may also be due to the calendar aging effects associated with FEC.

Rate capability test

In order to check whether the moderately loaded NVP/C cathodes with $1.2 \text{ mAh}/\text{cm}^2$ can deliver reasonable discharge capacities for rates up to 5 C, after the cell formation, an asymmetric rate capability test was performed in discharge direction with cells 2 and 4. The test protocol is specified in Table S3 and the results are shown in Figure 4. Compared to 0.5 C, a gradual reduction of the discharge capacity with increasing C-rate can be seen. Nevertheless, good discharge capacities are still achieved even at 5 C, where cell 2 and cell 4 deliver 82% respectively 76% of the discharge found at 0.5 C. This indicates that the loading of the NVP/C electrodes can possibly be increased significantly beyond the $1.2 \text{ mAh}/\text{cm}^2$ investigated herein.

After formation cycles, the cells were charged to 3.5 V and rested for 100 h at 25°C before the rate capability test. This pause might be plausible explanation for the high discrepancy of the discharge capacity of formation cycles (0.05 C, shown on the very left of figure 4) compared to the first cycles at 0.5 C in the FEC containing cell, which accounts for 15.4 mAh/g . In the FEC free cell, in contrast, the capacity only is reduced by 5.0 mAh/g from 88.6 (formation, 0.05 C) to 81.6 mAh/g at the beginning of the rate capability test (0.5 C). While the latter may well be explained by the different C-rates, the immense capacity loss of the FEC containing cell suggests ongoing

adverse FEC related reactions during storage at 25°C . Accordingly, the OCV voltage of cell 4 was 3.27 V at the beginning of the rate capability test, which is 5 mV below the 3.34 V measured in cell 2. However, it must be noted that these values interfere with overpotential effects, and that further experiments are necessary to properly understand this calendar aging behavior in detail.

Cycling stability test and internal resistances

As described in detail in the experimental section, after cell formation and rate capability tests continuous charge discharge cycles (0.5 CCCV charge, 0.5 C discharge) were carried out with check-up cycles at the beginning and after each 100 cycles (0.1 C charge and discharge). Figure 5 shows the discharge capacities (a, b), as well as the relative discharge capacities, referring to the first cycle of the cycling stability test (c, d). Just like from the formation cycles, it is evident that the N/P ratio directly influences the discharge capacity. An overbalancing of the HC anode leads to reduced starting capacities. The FEC free cells show decent cycling stabilities with similar relative capacity retentions of 89.5% and 88.6% after 1000 charge and discharge cycles. The FEC containing cells, in contrast, suffer from accelerated degradation, losing 20% of their starting capacity after roughly 1060 and 300 charge/discharge cycles, respectively. However, as stated before, no comparative data set is available for cell 4 due to early failure of the second cell. Hence, the relatively rapid loss of capacity in this case might have other causes, such as inadequate cell building.

In Figure 5(a and b), the discharge capacities determined in the check-up cycles are depicted as well. It becomes evident that the discrepancy to the discharge capacity at 0.5 C increases both with the overbalancing of the anode and with the additive FEC. This behavior might be due to the higher resistances of the overbalanced HC anodes and the SEIs formed in the FEC containing cells. The voltage profiles of the check-up cycles of cell 1 are depicted in Figure S1 and show now sign of increasing cell polarization. Another notable feature of all cell tests is that the check-up cycles positively influence the capacity of the subsequent cycles. This effect is even more pronounced in the cells with electrolyte B ($60 \text{ ppm H}_2\text{O}$), and therefore is discussed in the following section.

With the last update, the cell 1 had a remaining capacity of 85.1% after 1960 cycles and 234 days of testing. All results were achieved in coin cells, which are known to have reduced lifetimes compared to pouch cells.^[23] It can therefore be assumed that the degradation can still be significantly reduced by changing the cell format and that an excellent cycling stability should be possible based on NVP/C vs. HC cells with NaPF_6 in EC/PC as electrolyte. Likewise, it becomes evident that FEC, which doubtlessly extends the lifetime of NVP vs. Na cells,^[30] reduces the lifetime of NVP vs. HC cells and is therefore not a suitable additive in full-cells.

RiDC measurements at different stages of charge were performed at the beginning of the cycling stability test and then each after 100 charge and discharge cycles. The RiDC

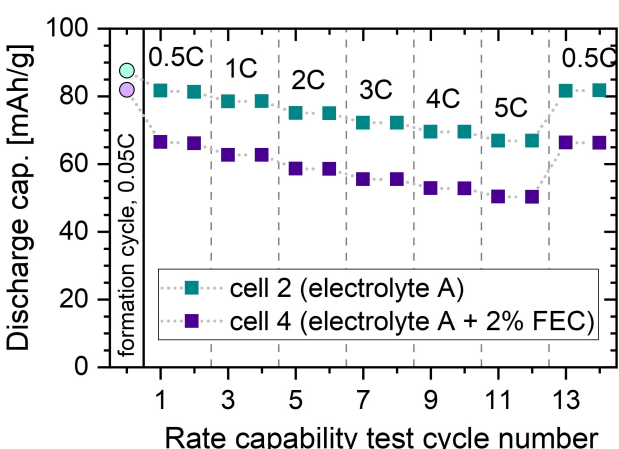


Figure 4. Discharge capacities found for C-rates of 0.5 to 5 C during the rate capability test (CR2032 coin cells, capacities related to the mass of NVP). For comparison, the discharge capacity obtained during cell formation was added on the left (circles). In between, the end of cell formation, cells were charged to 3.5 V and rest for 100 hours before starting the rate capability test.

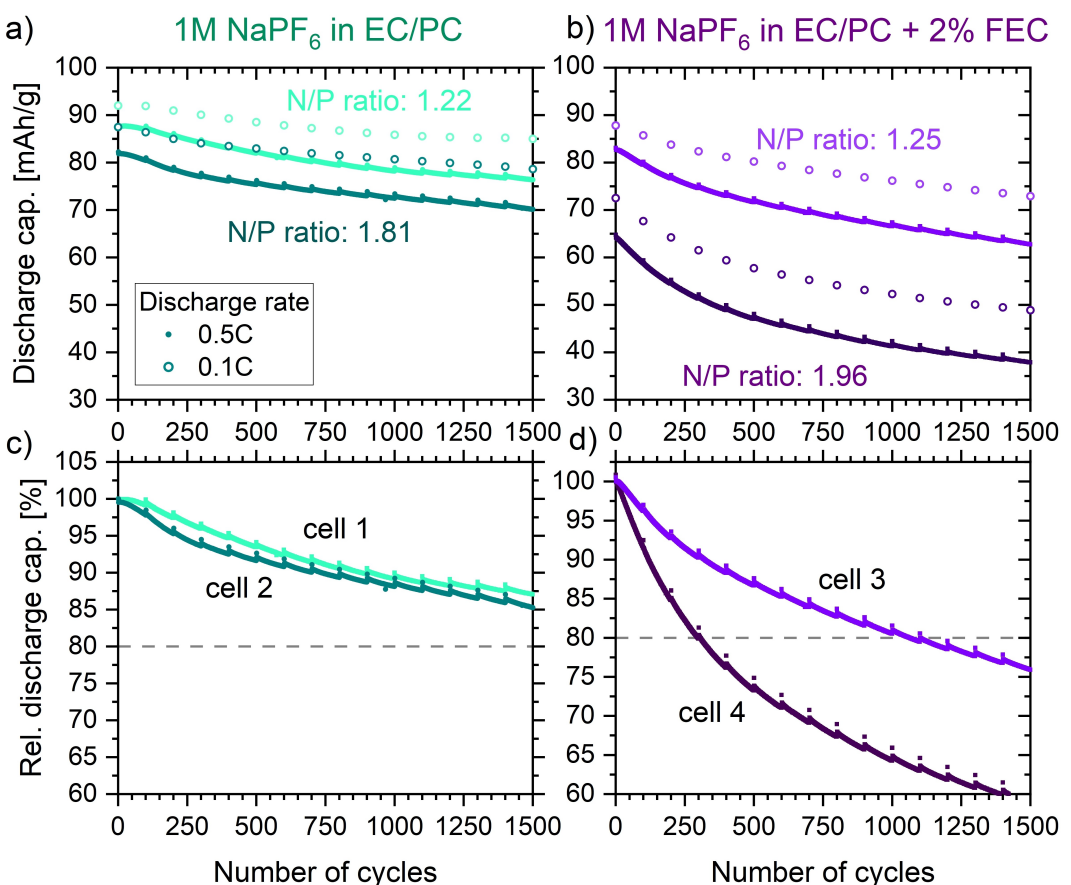


Figure 5. Cycling behavior of NVP/C vs. HC (CR2032 coin cells, capacities related to the mass of NVP) with different electrolytes and different N/P ratios at a C-rate of 0.5 C. a, b) specific discharge capacity and c, d) capacity retention, relative to the first discharge cycle at 0.5 C.

values varied between 20 and 160 Ω per coin cell. Based on an electrode surface of 2.01 cm^2 , the results were normalized, yielding the specific RiDC values shown in Figure 6. Again, the negative effect of FEC for the full-cells is evident. The cell resistances determined using the RiDC method are about 50% higher and tend to increase continuously over time. Remarkably, in the cells where NaPF_6 in EC/PC is used as electrolyte, the resistances hardly increase, which is a very encouraging finding with respect to the potential lifetime of the system. Regardless of the additive FEC and number of cycles, in all cells clearly the highest RiDC values were found at a state of charge of 10%. In contrast, similar and low values were consistently observed for 50% and 70% SOC. At 90% SOC, the resistance increases again noticeably and according to Mohsin *et al.*, the value should become significantly higher again in the fully charged state,^[22] which however was not part of our testing protocol.

Based on the assumption, that the loss of sodium inventory is the predominant cause for capacity loss, formal $\text{Na}_{3-x}\text{V}_2(\text{PO}_4)_3$ compositions after cell formation (20% Na^+ -loss) and of an aged cell (additional 20% Na^+ -loss) were calculated for different stages of charge. Together with the average vanadium oxidation states, the compositions are listed in Table 4. It becomes evident that the compositions at low SOC values are subject to greater changes than those at high SOC values,

which is clearly reflected in the variability of the RiDC values observed. Accordingly, in cell 4, which shows the largest increase in RiDC values, over 1500 cycles the resistance at SOC 90% only increases by $9\text{ }\Omega\text{cm}^2$, while the value for SOC 10% increases by $65\text{ }\Omega\text{cm}^2$. However, a simple and obvious relationship between SOC, RiDC and phase composition or formal vanadium oxidation states, respectively, cannot be seen. Hence for full and conclusive understanding of the SOC dependency of the RiDC values, further investigations, e.g., by means of impedance spectroscopy, seem to be necessary.

Nevertheless, as shown in Figure 6(a), in well-balanced, FEC free cells, the RiDC values were almost constant over 1500 cycles and almost 6 months of testing. This is a remarkable and promising result for long-term applications, as it indicates that such cells could potentially be operated for several years and many thousands of cycles. In this respect, the NVP/C vs. HC cells reveal a significantly higher stability even when compared to well-established Li-ion cell chemistries such as $\text{LiNi}_{0.33}\text{Mn}_{0.33}\text{Co}_{0.33}\text{O}_2$ vs. graphite. For the latter, a continuous increase of the RiDC values was consistently observed for very similar cell building parameters and with the same test method.^[23]

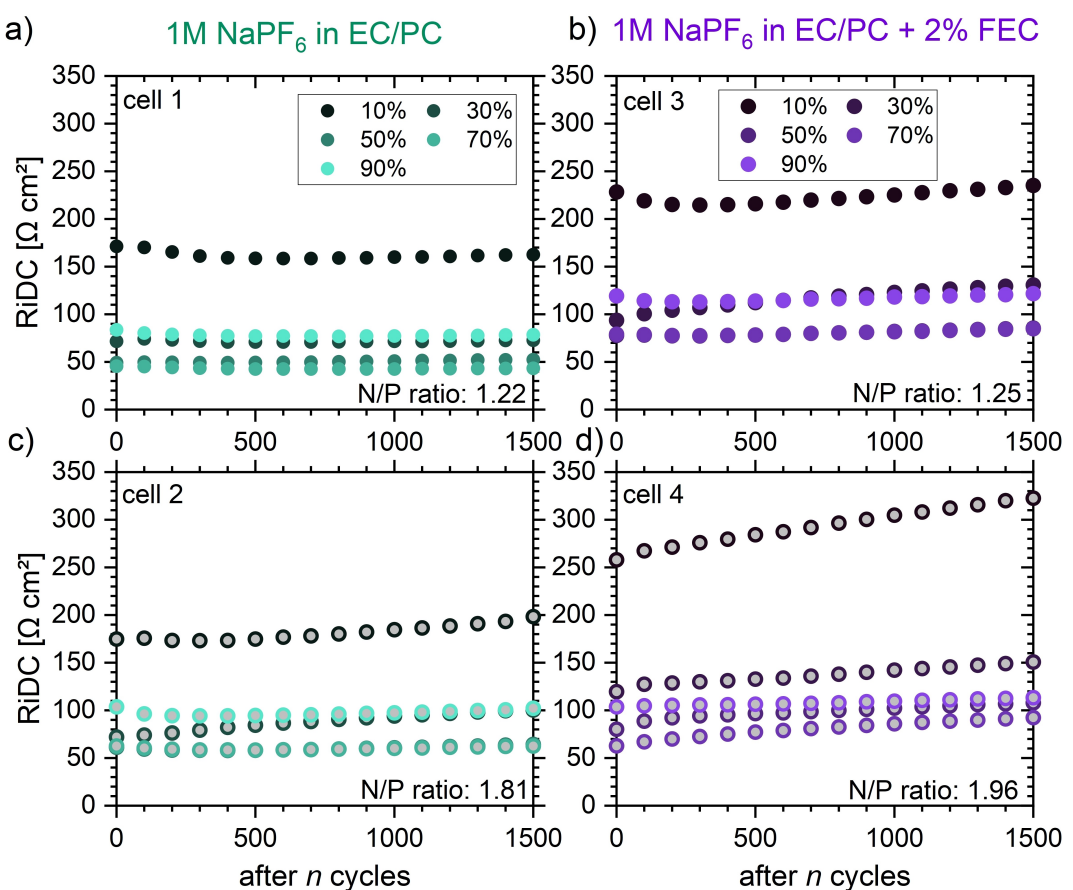


Figure 6. Direct current internal resistance determined from the check-up cycles during the cycling stability test for different states of charge. Both FEC and overbalancing of hard carbon negatively affect the RiDC values.

Table 4. Formal compositions of the cathode active material $\text{Na}_{3-x}\text{V}_2(\text{PO}_4)_3$ with the corresponding vanadium oxidation states (OS), based on the starting composition $\text{Na}_3\text{V}_2(\text{PO}_4)_3$ and two electrochemically active Na^+ ($0 < x < 2$). It is assumed that after formation, roughly 80% of the active Na^+ are still available ($0.4 < x < 2$), and at the end of the lifetime 80% thereof remain ($0.72 < x < 2$). The Δx values highlight the variation of the composition after formation and at the end of life for different stages of charges.

Condition	after formation (20% Na^+ -loss)			end of life (80% capacity, ret.)			
	x	Composition	OS(V)	x	Composition	OS(V)	Δx
SOC 0 %	0.40	$\text{Na}_{2.60}\text{V}_2(\text{PO}_4)_3$	3.20	0.72	$\text{Na}_{2.28}\text{V}_2(\text{PO}_4)_3$	3.36	0.32
SOC 10 %	0.56	$\text{Na}_{2.44}\text{V}_2(\text{PO}_4)_3$	3.28	0.84	$\text{Na}_{2.16}\text{V}_2(\text{PO}_4)_3$	3.42	0.28
SOC 30 %	0.88	$\text{Na}_{2.12}\text{V}_2(\text{PO}_4)_3$	3.44	1.10	$\text{Na}_{1.90}\text{V}_2(\text{PO}_4)_3$	3.55	0.22
SOC 50 %	1.20	$\text{Na}_{1.80}\text{V}_2(\text{PO}_4)_3$	3.60	1.36	$\text{Na}_{1.64}\text{V}_2(\text{PO}_4)_3$	3.68	0.16
SOC 70 %	1.52	$\text{Na}_{1.48}\text{V}_2(\text{PO}_4)_3$	3.76	1.62	$\text{Na}_{1.38}\text{V}_2(\text{PO}_4)_3$	3.81	0.10
SOC 90 %	1.84	$\text{Na}_{1.16}\text{V}_2(\text{PO}_4)_3$	3.92	1.87	$\text{Na}_{1.13}\text{V}_2(\text{PO}_4)_3$	3.94	0.03
SOC 100 %	2.00	$\text{Na}_{1.00}\text{V}_2(\text{PO}_4)_3$	4.00	2.00	$\text{Na}_{1.00}\text{V}_2(\text{PO}_4)_3$	4.00	0.00

Influence of electrolyte quality

In order to highlight the impact of the quality of the electrolyte (1 M NaPF_6 in EC/PC (w/w)), each two cells were built, in which all parameters were the same except for the use of electrolyte A vs. electrolyte B. Although both theoretically have the same composition (cf. Table 2), the purity of the individual components is higher in the case of electrolyte A. A clear deviation could also be found with regard to the water content, which

was determined to be <10 and 60 ppm in electrolyte A and B, respectively. Properties of the individual cells are listed in Table 3. As shown in Figure 7, the electrolyte quality significantly affects the first cycle of cell formation. As highlighted in Figure 7(b) at 3.0 V, an additional step can be seen in the charge profile. The charge capacity of the cell 5 was determined 111.2 mAh/g in the first cycle, which is in perfect agreement with the NVP capacity of 111.3 mAh/g observed in the half-cells (see above) and in good agreement with the charge capacities

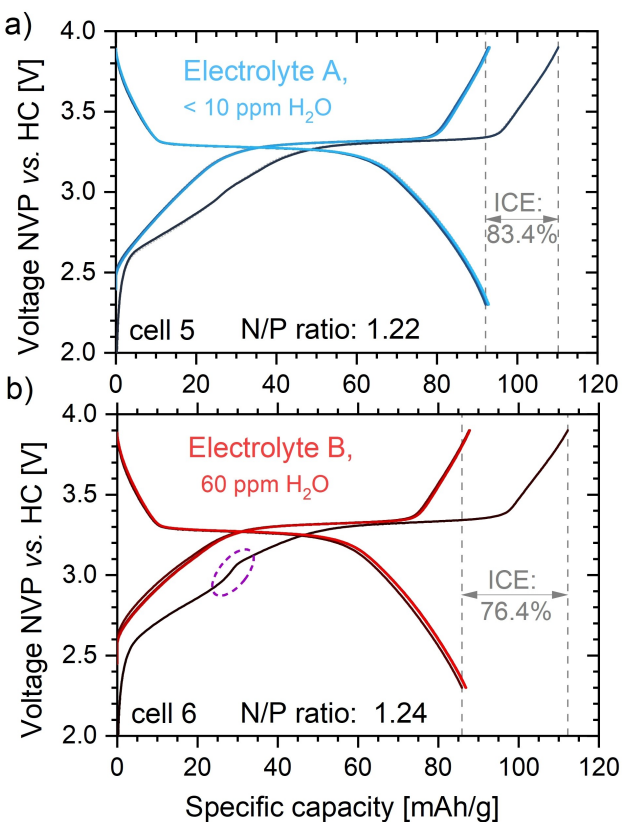


Figure 7. Influence of residual moisture in the electrolyte on voltage profiles of the formation cycles (4 cycles with 0.05 C, the line color becomes lighter with increasing cycle number). The N/P ratios values refer to the capacity of the NVP/C cathode vs. the capacity of the HC anode.

found in cells 1–4 (110.8–111.7 mAh/g). In moisture containing cell 6 in contrast, the first charge capacity is slightly increased to 112.3 mAh/g. Even though the excess capacity is small (0.6 mAh/g), this could be considered an indication that additional side reactions are taking place in the electrolyte in the presence of water. The ICE, which is closely related to the amount of sodium trapped in hard carbon and in the SEI, deviates significantly for electrolytes A and B. With the purer and dry electrolyte A, an ICE of 83.4% is observed, while the cell with the electrolyte B with 60 ppm water only yields 76.4%. In the subsequent formation cycles, the coulomb efficiencies in the water-containing cell 6 remain lower (98.9–99.0%) than in the cell with electrolyte A (99.6%–99.8%).

On the basis of the discharge capacity during the cycling stability tests, which are depicted in Figure 8(a and b), the impact of electrolyte quality becomes even more obvious. The cells with the rather dry electrolyte show greater capacity retention over the number of cycles than the cells with the water-containing electrolyte, especially over the first 500 cycles. The difference between the discharge capacity in the check-up cycle (0.1 C) and the continuous cycling (0.5 C) is significantly higher in the case of the water-containing electrolyte, which may be largely due to the internal resistances. The corresponding RiDC values for cells 5 and 6 determined during the cycling stability tests are shown in Figure 8(c and d). In the cells

containing water the resistances are clearly higher than those of the cells with the dry electrolyte and even exceed the values observed of the cells containing FEC (see above).

The determination of the water content by means of Karl-Fischer titration and the cell building to study the influence of moisture (cell 5 and 6) was carried out 3 months after the main investigation (cell 1–4). As expected, all cells built with electrolyte A (cell 1, 2 and 5) show a very similar formation behavior (cf. Figure 7a vs. 3a). The RiDC values obtained for cell 1 could likewise be reproduced. In cell 5, slightly higher values were observed, but no significant deviations (cf. Figure 8c vs. 6a). The reason for the somewhat greater capacity loss of cell 5 (Figure 8a) compared to cells 1 and 2 (Figure 5a), however, was surprising and cannot be explained straight away. A possible explanation could be that new coin cell sealing gaskets were used. The gaskets did not fit as good as usual and sometimes caused problems when closing the cells. Insufficient sealing of the cell housing is also supported by the observation that the formation cycles appeared normal and the somewhat faster degradation only became noticeable with time.

Pseudo-irreversible capacity losses

During this study, it was consistently observed that after the check-up cycles (0.1 C) and RiDC test, the discharge capacity of the subsequent cycles at 0.5 C were noticeably increased for roughly 10 (cells 1), to 50 cycles (cell 6). This becomes particularly evident from the serrated pattern of the 0.5 C discharge capacity shown in Figure 8(a and b), where data from the cell 6 with the moist electrolyte B is shown in red. However, to a weaker extend, all other cells show the same behavior (cf. Figure 5). Hence, it appears that after a slow charging and discharging process, the amount of electrochemically active sodium is increased for the subsequent cycles at the higher C-rate, but then is gradually lost again. The extend of these “pseudo-irreversible” capacity losses in each cell hardly changed over time and amounted to 0.6 mAh/g (cell 1) up to about 1.8 mAh/g (cell 6).

From the 0.5 C profiles in Figure 3 (dotted lines) it becomes also obvious, that CV phases which were applied in each charge step during the continuous cycling (0.5 C charge with CV step until 0.05 C; 0.5 C discharge), did not make any significant contribution to the overall charge capacity of the NVP/C vs. HC cells. Upon a closer inspection, it is therefore likely that the reduced discharge capacities at 0.5 C can be explained by the circumstance, that the full-cells were not fully discharged at 0.5 C in the voltage window of 3.9 to 2.3 V. This implies that additional sodium remains pseudo irreversibly trapped in the HC anode during standard cycling. This assumption supported by the fact that the charge capacities in the check-up cycles at 0.1 C, which were performed after 100 cycles at 0.5 C, are reduced compared to the following discharge capacities at 0.1 C, which can be seen in Figure S1. Accordingly, coulomb efficiencies of ~107% are observed in these check-up cycles. During standard cycling at 0.5 C in contrast, reduced coulombic efficiencies were observed which then increased until dropping

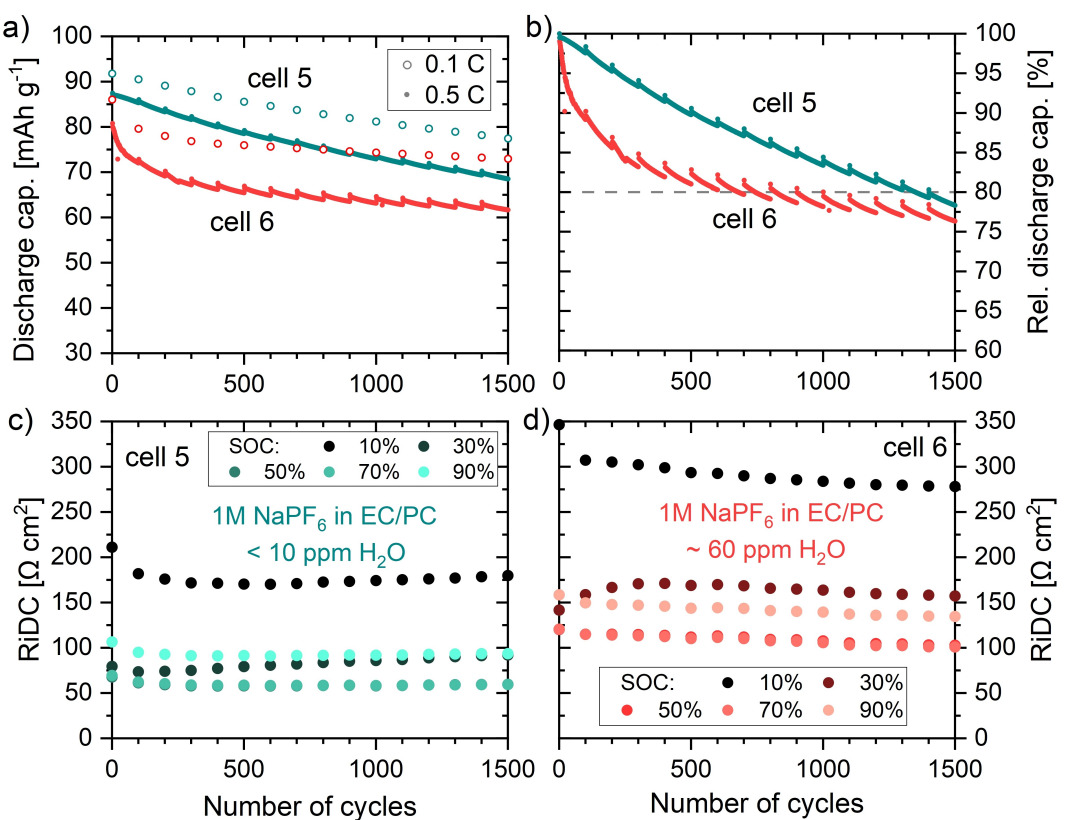


Figure 8. a) Discharge capacity of NVP/C vs. HC full-cells with electrolyte A (cell 5) and electrolyte B (cell 6). b) Discharge capacity relative to the first discharge cycle at 0.5 C. c, d) Results of the RiDC measurements of the check-up cycles at different stages of charge.

again after the next check-up cycle. An example of this behavior is shown in Figure S2, where a mean coulomb efficiency was fitted over the data points. Regarding the measurement accuracy, however, it must be clearly noted that the test hardware used here reaches its limits, as the absolute CE values and the results for individual cycles are not very reliable and do not allow for further quantitative analysis.

Nevertheless, based on the relative increase in CE values during the standard cycling and the high CE values of the check-up cycles, it seems reasonable to assume that slow discharge processes of the NVP/C vs. HC batteries are capable of reactivating some “lost” sodium trapped in the HC anode, which then is lost again over time. It is conceivable that the problem could be reduced by decreasing the lower voltage limit or using a CV phase for the discharge step as well.

Conclusions and Outlook

Our study shows that based on NVP/C cathodes and hard carbon anodes, sodium-ion batteries with excellent cycling stabilities (> 85% capacity retention over 1960 cycles) can be realized using EC/PC based electrolyte and the conducting salt NaPF_6 . Manually built coin cells were investigated, and it can be assumed that with industrial manufacturing technology and in larger cell formats, even significantly better cycling stabilities can be achieved. Based on a rate capability test, it was shown

that the electrodes with capacities of $\sim 1.2 \text{ mAh/cm}^2$ can still provide considerable discharge capacities even at 5 C (> 75% compared to 0.5 C), which indicates that the areal capacity of the NVP/C and HC electrodes may still be significantly increased. The N/P ratio hardly affects the cell degradation. However, due to irreversible loss of active sodium within HC anodes, overbalanced anodes lead to even greater losses of the overall cell capacity. Therefore, it is crucial to determine the capacities of the individual electrodes at first and then to balance them properly. Another issue for the cycle life of NVP/C vs. HC cells is the electrolyte quality. It has been shown that the use of an electrolyte made of less pure solvents and containing 60 ppm of water, has a negative effect on cell formation, capacity and lifetime. For the full-cells with highest capacity retention investigated, the N/P ratio was 1.22 and 1.81, which led to discharge capacities of 94 mAh and 87 mAh per g NVP, respectively, which is a decent result for NVP/C vs. HC full-cells. However, these values are still significantly reduced compared to the NVP capacity of 111 mAh/g obtained in half-cell configuration. Hence, even with optimal balancing, achieving full-cell capacities of $> 100 \text{ mAh/g}$ seems to be a great challenge. Therefore, based on the current knowledge, appropriate pre-sodiation strategies seem inevitable and simple and scalable processes need to be developed. The additive FEC, which doubtlessly increases the life-time of NVP/C vs. sodium metal half-cells, causes detrimental effects within NVP/C vs. HC full-cells. Both, loss of active sodium and

accelerated capacity decay are observed. FEC seems to have a negative effect on the SEI formation and causes higher internal resistances, which increase continuously during cell aging. The internal resistances in the cells containing NaPF_6 in EC/PC exclusively, in contrast are significantly lower and hardly increase even after 12 months of testing and 3000 full cycles. This is a highly promising finding, as it indicates that it might be possible to build NVP/C vs. HC cells with outstanding cycling stability that can last for years if not for decades, which is decisive for the assessment of the sustainability of the SIB technology.

Author Contributions

Conceptualization: A.S., C.M., P.St. (equal), A.H. (supporting). **Methodology:** A.S., C.M., P.St. (equal). **Investigation:** P.St. (lead), A.H., C.M., J.K., M.H., (equal.), J.B. (supporting). **Resources:** A.H., A.S., J.B. (equal), P.Sch., W.S. (supp.). **Writing – Original Draft:** P.St. (lead), A.S., C.M., J.B., J.K. (supporting). **Writing – Review & Editing:** A.S., P.St. (equal), A.H., C.M., J.B., J.K., M.H., P.Sch., W.S. (supporting). **Visualization:** P.St. (lead). **Validation:** P.St. (lead), A.S., C.M. (supporting). **Supervision:** A.S., P.St. (equal). **Project administration:** A.S. (lead); **Funding acquisition:** A.S. (lead)

Acknowledgements

We thank Karsten Schmidt for the execution of the Karl-Fischer Titration and Marcus Müller for calendering the electrodes. Further we would like to thank Steffen Jokisch and Robert Löwe for the support in carrying out and evaluating the cell test. This work contributes to the research performed at CELEST (Center for Electrochemical Energy Storage Ulm-Karlsruhe) and was funded by the German Research Foundation (DFG) under Project ID 390874152 (POLIS Cluster of Excellence, EXC 2154). Open Access funding enabled and organized by Projekt DEAL.

Conflict of Interests

The authors declare no conflict of interest.

Data Availability Statement

The authors declare that the data supporting the findings of this study are available within the paper and the Supplementary Information file. The battery cycling data (and the corresponding masses of the active materials of the corresponding cells), are available in the Zenodo repository with the DOI: 10.5281/zenodo.10040915.

Keywords: cycling stability • full-cell • hard carbon • $\text{Na}_3\text{V}_2(\text{PO}_4)_3$ • sodium-ion battery

- [1] B. L. Cushing, J. B. Goodenough, *J. Solid State Chem.* **2001**, *162*, 176.
- [2] L. S. Plashnitsa, E. Kobayashi, Y. Noguchi, S. Okada, J. Yamaki, *J. Electrochem. Soc.* **2010**, *157*, A536.
- [3] Z. Jian, L. Zhao, H. Pan, Y.-S. Hu, H. Li, W. Chen, L. Chen, *Electrochim. Commun.* **2012**, *14*, 86.
- [4] K. Saravanan, C. W. Mason, A. Rudola, K. H. Wong, P. Balaya, *Adv. Energy Mater.* **2013**, *3*, 444.
- [5] X. Zhang, X. Rui, D. Chen, H. Tan, D. Yang, S. Huang, Y. Yu, *Nanoscale* **2019**, *11*, 2556.
- [6] G. Chen, Q. Huang, T. Wu, L. Lu, *Adv. Funct. Mater.* **2020**, *30*, 2001289.
- [7] Z. Jian, Y. Sun, X. Ji, *Chem. Commun. (Camb.)* **2015**, *51*, 6381.
- [8] D. Wang, N. Chen, M. Li, C. Wang, H. Ehrenberg, X. Bie, Y. Wei, G. Chen, F. Du, *J. Mater. Chem. A* **2015**, *3*, 8636.
- [9] P. L. Mani Kanta, N. L. Priya, P. Oza, M. Venkatesh, S. K. Yadav, B. Das, G. Sundararajan, R. Gopalan, *ACS Appl. Energ. Mater.* **2021**, *4*, 12581.
- [10] Y. Liu, X. Wu, A. Moezz, Z. Peng, Y. Xia, D. Zhao, J. Liu, W. Li, *Adv. Energy Mater.* **2023**, *13*, 2203283.
- [11] a) P. Ge, M. Fouletier, *Solid State Ionics* **1988**, *28–30*, 1172; b) B. Jache, P. Adelhelm, *Angew. Chem. Int. Ed.* **2014**, *53*, 10169; c) M. Goktas, C. Bolli, E. J. Berg, P. Novák, K. Pollok, F. Langenhorst, M. v. Roeder, O. Lenchuk, D. Mollenhauer, P. Adelhelm, *Adv. Energy Mater.* **2018**, *8*, 1702724.
- [12] H. Liu, M. Baumann, X. Dou, J. Klemens, L. Schneider, A.-K. Wurba, M. Häringen, P. Scharfer, H. Ehrenberg, W. Schabel, et al., *J. Energy Storage* **2022**, *56*, 105964.
- [13] F. Xie, Z. Xu, Z. Guo, M.-M. Titirici, *Prog. Energy* **2020**, *2*, 42002.
- [14] Y. Wan, Y. Liu, D. Chao, W. Li, D. Zhao, *Nano Mater. Sci.* **2023**, *5*, 189–201.
- [15] H. Au, H. Alptekin, A. C. S. Jensen, E. Olsson, C. A. O’Keefe, T. Smith, M. Crespo-Ribadeneyra, T. F. Headen, C. P. Grey, Q. Cai, et al., *Energy Environ. Sci.* **2020**, *13*, 3469.
- [16] Y.-B. Niu, Y.-J. Guo, Y.-X. Yin, S.-Y. Zhang, T. Wang, P. Wang, S. Xin, Y.-G. Guo, *Adv. Mater.* **2020**, *32*, e2001419.
- [17] D. Shanmukaraj, K. Kretschmer, T. Sahu, W. Bao, T. Rojo, G. Wang, M. Armand, *ChemSusChem* **2018**, *11*, 3286.
- [18] M. Baumann, M. Häringen, M. Schmidt, L. Schneider, J. F. Peters, W. Bauer, J. R. Binder, M. Weil, *Adv. Energy Mater.* **2022**, *12*, 2202636.
- [19] Vivienne HALLEUX, *New EU regulatory framework for batteries: Setting sustainability requirements*, EPRI: European Parliamentary Research Service, **2021**.
- [20] T. Akçay, M. Häringen, K. Pfeifer, J. Anhalt, J. R. Binder, S. Dsoke, D. Kramer, R. Mönig, *ACS Appl. Energ. Mater.* **2021**, *4*, 12688.
- [21] C. V. Manohar, T. C. Mendes, M. Kar, D. Wang, C. Xiao, M. Forsyth, S. Mitra, D. R. MacFarlane, *Chem. Commun.* **2018**, *54*, 3500.
- [22] I. U. Mohsin, L. Schneider, M. Häringen, C. Ziebert, M. Rohde, W. Bauer, H. Ehrenberg, H. J. Seifert, *J. Power Sources* **2022**, *545*, 231901.
- [23] A. Smith, P. Stüble, L. Leuthner, A. Hofmann, F. Jeschull, L. Mereacre, *Batteries & Supercaps* **2023**, *6*.
- [24] P. Stüble, M. Müller, T. Bergfeldt, J. R. Binder, A. Hofmann, *Adv. Sci.* **2023**, *10*, e2301874.
- [25] M. J. Aragón, P. Lavela, G. F. Ortiz, R. Alcántara, J. L. Tirado, *Inorg. Chem.* **2017**, *56*, 11845.
- [26] M. Liu, J. Zhang, S. Guo, B. Wang, Y. Shen, X. Ai, H. Yang, J. Qian, *ACS Appl. Mater. Interfaces* **2020**, *12*, 17620.
- [27] L. Zhao, H. Zhao, J. Wang, Y. Zhang, Z. Li, Z. Du, K. Świerczek, Y. Hou, *ACS Appl. Mater. Interfaces* **2021**, *13*, 8445.
- [28] K. Subramanyan, M. Akshay, Y.-S. Lee, V. Aravindan, *Adv. Mater. Technol.* **2022**, *7*, 2200399.
- [29] X. Yin, Y. Zhao, X. Wang, X. Feng, Z. Lu, Y. Li, H. Long, J. Wang, J. Ning, J. Zhang, *Small* **2022**, *18*, e2105568.
- [30] J. Zhang, J. Gai, K. Song, W. Chen, *Cell Rep. Phys. Sci.* **2022**, *3*, 100868.
- [31] X. Jiang, X. Liu, Z. Zeng, L. Xiao, X. Ai, H. Yang, Y. Cao, *iScience* **2018**, *10*, 114.
- [32] B. Xiao, F. A. Soto, M. Gu, K. S. Han, J. Song, H. Wang, M. H. Engelhard, V. Murugesan, K. T. Mueller, D. Reed, et al., *Adv. Energy Mater.* **2018**, *8*, 1801441.
- [33] W. Zhang, F. Zeng, H. Huang, Y. Yu, M. Xu, L. Xing, W. Li, *Nano Res.* **2023**, *16*, 3823.
- [34] J. Klemens, L. Schneider, E. C. Herbst, N. Bohn, M. Müller, W. Bauer, P. Scharfer, W. Schabel, *Energy Technol.* **2022**, *10*, 2100985.
- [35] J. Klemens, D. Burger, L. Schneider, S. Spiegel, M. Müller, N. Bohn, W. Bauer, H. Ehrenberg, P. Scharfer, W. Schabel, *Energy Technol.* **2023**, *11*, 2300267.
- [36] J. Klemens, L. Schneider, D. Burger, N. Zimmerer, M. Müller, W. Bauer, H. Ehrenberg, P. Scharfer, W. Schabel, *Energy Technol.* **2023**, *11*, 2300338.
- [37] C. Müller, Z. Wang, A. Hofmann, P. Stüble, X. Liu-Théato, J. Klemens, A. Smith, *Batteries & Supercaps* **2023**, *6*, e202300322.

- [38] a) A. Ponrouch, E. Marchante, M. Courty, J.-M. Tarascon, M. R. Palacín, *Energy Environ. Sci.* **2012**, *5*, 8572; b) K. Chayambuka, R. Cardinaels, K. L. Gering, L. Raijmakers, G. Mulder, D. L. Danilov, P. H. Notten, *J. Power Sources* **2021**, *516*, 230658; c) A. Hofmann, Z. Wang, S. P. Bautista, M. Weil, F. Müller, R. Löwe, L. Schneider, I. U. Mohsin, T. Hanemann, *Electrochim. Acta* **2022**, *403*, 139670; d) G. G. Eshetu, S. Gruegeon, H. Kim, S. Jeong, L. Wu, G. Gachot, S. Laruelle, M. Armand, S. Passerini, *ChemSusChem* **2016**, *9*, 462.
- [39] J. Fondard, E. Irisarri, C. Courrèges, M. R. Palacin, A. Ponrouch, R. Dedryvère, *J. Electrochem. Soc.* **2020**, *167*, 70526.

Manuscript received: October 27, 2023

Revised manuscript received: November 24, 2023

Version of record online: December 11, 2023
